STRONG VARIABILITY OF OVERLAPPING IRON BROAD ABSORPTION LINES IN FIVE RADIO-SELECTED QUASARS

Shaohua Zhang[1], Hongyan Zhou[1,2], Tinggui Wang[2], Huiyuan Wang[2], Xiheng Shi[1,3], Bo Liu[1,2], Wenjuan Liu[1,2], Zhenzhen Li[1,2], and Shufen Wang[1,2]

[1] Polar Research Institute of China, 451 Jinqiao Road, Shanghai, 200136, China; zhangshaohua@pric.org.cn, zhouhongyan@pric.org.cn
[2] Key Laboratory for Research in Galaxies and Cosmology, Department of Astronomy, University of Science and Technology of China, Chinese Academy of Sciences, Hefei, Anhui, 230026, China
[3] National Astronomical Observatories, Chinese Academy of Sciences, Beijing 100012, China

ABSTRACT

We present a study of the variability of broad absorption lines (BALs) in a uniformly radio-selected sample of 28 BAL quasars using the archival data from the FIRST Bright Quasar Survey and the Sloan Digital Sky Survey as well as data we obtained ourselves, covering timescales of $\sim 1 - 10$ yr in the quasar rest frame. To our surprise, five quasars exhibiting strong variations all belong to a special subclass of "overlapping-trough" iron low-ionization BAL (OFeLoBAL) quasars; however, four other non-overlapping FeLoBALs (non-OFeLoBALs) are invariant, except in one case with a weak change in optical depth. Meanwhile, we also identify six typical variations of high-ionization and low-ionization BALs in this BAL quasar sample. Photoionization models suggest that OFeLoBALs are formed in relatively dense ($n_e > 10^6 \, \mathrm{cm^{-3}}$) outflows at distances from the continuum source that range from the subparsec scale to dozens of parsecs. These formation conditions differ from those of non-OFeLoBALs, which are likely produced by low-density gas located at distances of hundreds to thousands of parsecs. Thus, OFeLoBALs and non-OFeLoBALs, i.e., FeLoBALs with/without strong BAL variations, may represent the bimodality of Fe II absorption; the former are located in active galactic nucleus environments rather than in the host galaxy. We suggest that a high density and a small distance are the necessary conditions for the creation of OFeLoBALs. As suggested in the literature, strong BAL variability is possibly attributable to variability in the covering factor of the BAL regions caused by clouds transiting across the line of sight rather than to variations in ionization.

Key words: galaxies: active – quasars: absorption lines – quasars: general

1. INTRODUCTION

Broad absorption lines (BALs; Weymann et al. 1991) are the most readily apparent signature of outflowing gas. Strong outflows are believed to be one of the most important feedback processes connecting central supermassive black holes (SMBHs) to their host galaxies. However, the detailed physics of these outflows is not well understood. Studies of BALs can provide a useful approach to placing constraints on the physical properties of outflows to further understand the overall picture of galaxy evolution and the connection between SMBHs and their surrounding hosts in quasars.

BALs are observed in the blueward of emission lines with a wide range of blueshifted velocities (up to $\sim 0.2c$) and broad widths (at least $2000 \, \mathrm{km \, s^{-1}}$; Weymann et al. 1991). Based on the species of absorption, BALs are divided into three subclasses, i.e., high-ionization BALs (HiBALs), low-ionization BALs (LoBALs), and iron low-ionization BALs (FeLoBALs; e.g., Hall et al. 2002). In addition to the BALs of the high-ionization species (e.g., C IV) in HiBALs, and those of the low-ionization species (e.g., Mg II and Al III) in LoBALs, FeLoBALs also show BALs in ground and excited of states Fe II and/or Fe III (Hazard et al. 1987; Becker et al. 1997). Statistical studies indicate that approximately 10–20% of quasars exhibit BALs, and $\sim 15\%$ of BAL quasars are detected as LoBAL quasars; by contrast, FeLoBALs are the rarest subclass, appearing in at most $\sim 1\%$ of BAL quasars (e.g., Weymann et al. 1991; Reichard et al. 2003; Trump et al. 2006; Gibson et al. 2009; Zhang et al. 2010).

BAL variability studies provide one method of assessing BAL structures, locations and dynamics, and the results of such studies can potentially constrain the physical mechanisms responsible for outflows. In principle, the observed BAL variability could be explained by variations in the ionization parameter (e.g., Trevese et al. 2013), clouds transiting across the line of sight (e.g., Hall et al. 2011) or a combination of processes driven by these two factors. Recently, time variability in individual sources or samples with multi-epoch observations has been reported for HiBALs (e.g., Lundgren et al. 2007; Capellupo et al. 2012, 2013; Filiz Ak et al. 2013; Joshi et al. 2014), for LoBALs (Zhang et al. 2011; Vivek et al. 2014), and for FeLoBALs (Vivek et al. 2012; McGraw et al. 2014). Absorption-line variability is perhaps more common within shallower and higher-velocity troughs (e.g., Capellupo et al. 2011) on longer timescales (e.g., Gibson et al. 2008, 2010; Capellupo et al. 2011); occasionally, absorption lines are even observed to disappear completely (e.g., Hall et al. 2011; Filiz Ak et al. 2012). However, there has been no study to date that has compared variability among different BAL subclasses.

Radio observations could be used to constrain BAL orientations through investigations of radio variability, spectral index and morphology (Zhou et al. 2006; DiPompeo et al. 2012 and references therein). To date, only one BAL variability investigation of radio-loud (RL) BAL quasars has been performed by Welling et al. (2014). They found that the BAL variability did not significantly depend on either radio luminosity or radio-loudness; however, there was tentative

evidence of greater fractional BAL variability within lobe-dominated RL quasars. The FIRST Bright Quasar Survey[4] (FBQS; White et al. 2000) provided a uniform radio-selected sample of 29 definite and tentative BAL quasars (Becker et al. 2000). Using the data collected in this survey, it is possible to perform a statistical comparison of BAL variability among radio-selected BAL subclasses.

This paper is organized as follows: Section 2 describes the multi-epoch observations of the sample, Section 3 presents the BAL variability, and Section 4 summarizes and discusses the implications. Throughout this paper, we adopt the CDM "concordance" cosmology with $H0 = 70 \, \mathrm{km \, s^{-1} \, Mpc^{-1}}$, $\Omega_m = 0.3$, and $\Omega_\Lambda = 0.7$.

2. SAMPLE SELECTION AND OBSERVATIONS

White et al. (2000) presented the optical spectra of 636 quasars in the FBQS distributed over 2682 $\mathrm{deg^2}$ in their Table 2 and Figure 16. These quasar data form a heterogeneous set, collected at five different observatories between 1996 and 1998. The maximum coverage of the spectroscopic instruments is from ~3600 to 10,000 Å with a ~4–10 Å resolution. We checked these spectra and adjusted the BAL quasar sample identified by White et al. (2000) and Becker et al. (2000). Two tentative BALs were rejected,[5] one quasar (FBQS J105528.808 +312411.65) was reclassified as a FeLoBAL quasar, and four LoBALs were reclassified as HiBALs and FeLoBALs. The final working sample contained 28 BALs, including 15 HiBALs, 4 LoBALs, and 9 FeLoBALs (Table 1). Of these, five FeLoBALs were discovered to exhibit abrupt dropes in flux, yielding almost no continuum windows below Mg II and causing overlapping Fe II troughs; these were classified as "overlapping-trough" FeLoBALs (OFeLoBALs).

We searched the repeated spectroscopic observations from the Sloan Digital Sky Survey (SDSS; York et al. 2000) databases that have been obtained over the past 12 yr, from 2000 May to 2012 July. In the SDSS Seventh Data Release (DR7; Abazajian et al. 2009), 27 cases have spectra of higher spectral resolution. The DR7 spectrographs cover the wavelength range from 3800 to 9200 Å with a resolution of ~1.5 Å at 6500 Å, which is nearly coincident with the wavelength coverage of the FBQS. In addition, 16 cases were observed with the Baryon Oscillation Spectroscopic Survey (BOSS) spectrographs, whose spectral resolution varies from ~1300 at 3600 Å to 2500 at 10,000 Å (Smee et al. 2013). These new repeated observations were released as part of the SDSS Tenth Data Release (DR10; Ahn et al. 2014).

Meanwhile, we performed follow-up observations of FBQS J072831.6+402615 and J105528.8+312411 using the Opto-mechanics Research (OMR) spectrograph of the Xinglong 2.16 m telescope of the National Astronomical Observatories of China (NAOC) on 2009 March 24. A 200 Å $\mathrm{mm^{-1}}$ dispersion grating and a PI 1340 × 400 CCD detector were used to cover a wavelength range of 3800–8500 Å at a 4 Å resolution. Two exposures of 45 and 60 minute each were acquired for both cases. A slit width of 2″5 was chosen to match the typical seeing disk. For FBQS J072831.6+402615, an additional spectroscopic observation was performed on 2013 December

12, using the Yunnan Faint Object Spectrograph and Camera instrument of the Lijiang 2.4 m telescope of the Yunnan Astronomical Observatories (YNAO). The blue-band grism, G14, provided a wavelength coverage from ~3500 to 7500 Å with a spectral resolving power of 1337. The typical seeing was around 1″5, the slit width was 2″0, and one exposure of 30 minute was acquired. The follow-up spectroscopic data were reduced using the IRAF longslit and echelle packages.

3. BAL VARIABILITY

The repeated spectra, which were converted to the quasar rest frame using the redshifts reported in White et al. (2000), cannot be directly compared with the FBQS spectra because of the absolute flux calibration or continuum variability. Thus, we used a power-law form ($\propto \lambda^{\alpha_\lambda}$) to scale the repeated spectra to match the FBQS spectra, thereby masking the obvious absorption troughs. However, we found that the power-law indexes were equal to zero in most cases. The large time intervals between the FBQS and repeated spectroscopic observations are comparable to the expected time scale for outflow rearrangement, thus making the detection of variability more likely. We restricted our focus to BAL variability, while neglecting both emission-line variability and residual-continuum variability.

Through spectral comparisons among two or three epochs, one can clearly identify variable absorption troughs in 12 BAL quasars, including five "strong" variations (Figures 1, 2, and 3) and seven "typical" variations[6] (Figure 4). In this work, a typical variation refers to a small-amplitude velocity structure and/or optical-depth change of the absorption trough; by contrast, a strong variation is defined as an extremely large and continuous change. In the figures, the FBQS spectra are plotted in black, and the repeated spectra are plotted in red and green. Table 1 suggests that BAL variability does not tend to increase with greater radio-loudness or luminosity. This is consistent with the study of the BAL variability of RL quasars performed by Welling et al. (2014), in which no evidence of any correlation of the radio-loudness and luminosity with the BAL variability was found; the BAL variations in RL BAL quasars appear to occur in a similar manner as those in radio-quiet BAL quasars. When we further explore the subtypes and structures of the BALs, we find that the trends of BAL variability are completely different for HiBALs, LoBALs, FeLoBALs, and OFeLoBALs. Typical BAL variations are detected in the first three subtypes; however, intriguingly, all five instances of strong variations are detected in OFeLoBALs. Thus, we focus on strong variability in this work. In Figures 1, 2, and 3, we present the difference spectra for strong variations. The difference spectra are the observed spectra for the corresponding MJDs normalized to the highest fluxes among the multi-epoch observations; these spectra reveal the absorption-line variability more clearly. Next, we analyze the properties of these cases.

As shown in Figure 1, FBQS J072831.6+402615 and J140806.2+305448 (first reported in Hall et al. 2011) exhibit the strong weakening and even disappearance of the Fe II absorption lines. We providentially observed the process of transformation from an OFeLoBAL quasar to a non-BAL

Table 1
The Properties of FBQS BAL Quasars

Name (FBQS)	z	M_B	$\log L_R$	$\log R^*$	α	MJD	MJD-plate-fiber	MJD-plate-fiber	Δt^{1-2}	Δt^{1-3}	Σ_V	σ_V	Type
(1)	(2)	(3)	(4)	(5)	(6)	(7)	(8)	(9)	(10)	(11)	(12)	(13)	(14)
J072418.4+415914	1.552	−26.6	32.6	1.52	+0.0	51146	53312-1865-261	⋯	2.31	⋯	⋯	⋯	LoBAL[a]
J072831.6+402615	0.656	−28.0	32.2	0.57	−1.1	50774	54915	56654	6.85	9.73	0.09	0.06	OFeLoBAL[b]
J080901.3+275341	1.511	−27.7	31.9	0.40	⋯	50851	52618-0930-135	55858-4457-0512	1.93	5.46	⋯	⋯	HiBAL
J084044.4+363328	1.230	−27.2	31.7	0.39	−0.2	50838	52320-0864-149	⋯	1.82	⋯	⋯	⋯	FeLoBAL
J091044.9+261253	2.920	−27.6	33.1	1.65	−0.5	51160	53415-2087-352	⋯	1.58	⋯	⋯	⋯	HiBAL
J091328.2+394444	1.580	−27.4	32.1	0.65	−0.6	50094	52707-0937-569	⋯	2.77	⋯	⋯	⋯	HiBAL
J093403.9+315331	2.419	−28.5	32.8	0.88	−0.2	50401	53386-1941-600	⋯	2.39	⋯	⋯	⋯	HiBAL[a]
J094602.2+274407	1.748	−27.9	32.4	0.74	<−1.5	50466	53385-1944-026	⋯	2.91	⋯	⋯	⋯	HiBAL
J095707.3+235625	1.995	−27.4	34.1	2.64	−0.6	51172	53737-2298-409	⋯	2.35	⋯	⋯	⋯	HiBAL
J103110.6+395322	1.082	−25.8	31.8	1.04	−0.2	50465	52998-1428-608	⋯	3.33	⋯	⋯	⋯	LoBAL
J104459.5+365605	0.701	−26.2	32.2	1.30	−0.5	50486	53463-2090-329	55615-4635-0704	4.79	8.26	⋯	⋯	FeLoBAL
J105427.1+253600	2.400	−28.0	32.6	0.91	−0.5	50486	53793-2357-227	⋯	2.66	⋯	⋯	⋯	LoBAL[a]
J105528.8+312411	0.558	−23.9	31.7	1.68	⋯	50597	53711-2026-085	54915	5.48	7.59	0.07	0.00	OFeLoBAL[b]
J120051.5+350831	1.700	−29.1	32.1	0.01	−0.8	50586	53469-2099-606	55648-4650-0052	2.93	5.14	⋯	⋯	HiBAL
J121442.3+280329	0.698	−26.3	31.5	2.08	−0.8	50549	53823-2229-557	⋯	5.28	⋯	⋯	⋯	FeLoBAL
J130425.5+421009	1.916	−28.7	32.1	1.62	+0.7	50495	53119-1458-579	55681-4704-0881	2.47	4.87	⋯	⋯	HiBAL[a]
J131213.5+231958	1.508	−27.4	33.3	1.30	−0.8	50585	54507-2651-380	56098-5977-0326	4.28	6.02	⋯	⋯	HiBAL
J132422.5+245222	2.357	−27.4	32.8	1.32	−0.7	51009	54524-2664-537	56096-0186-0186	2.87	4.15	⋯	⋯	HiBAL
J140800.4+345125	1.215	−26.3	32.0	1.01	−0.6	50486	53471-1839-377	55268-3855-0386	3.69	5.91	0.08	0.00	OFeLoBAL[b]
J140806.2+305448	0.842	−24.8	31.7	1.33	−0.7	50601	53795-2125-236	55276-3862-0124	4.75	6.95	0.07	0.00	OFeLoBAL[b]
J141334.4+421201	2.810	−28.3	33.5	1.69	−0.2	50586	52823-1347-539	56093-6059-0438	1.61	3.96	⋯	⋯	HiBAL
J142013.0+253403	2.240	−27.9	32.1	0.49	−1.1	50596	53859-2127-011	56096-6015-0432	2.76	4.65	⋯	⋯	HiBAL[a]
J142703.6+270940	1.170	−25.6	32.0	1.27	−0.7	50616	53876-2134-256	56067-6018-0412	4.12	6.88	⋯	⋯	FeLoBAL[a]
J152314.4+375928	1.344	−26.5	31.9	0.78	−0.6	50245	53470-1400-450	56045-4979-0218	3.77	6.78	⋯	⋯	HiBAL
J152350.4+391404	0.657	−26.3	31.6	0.61	−0.4	50507	52765-1293-234	56045-4979-0804	3.73	9.12	0.06	0.00	OFeLoBAL[b]
J160354.2+300208	2.026	−27.9	33.7	2.04	−0.6	50507	53496-1578-534	55707-5009-0569	2.71	4.71	⋯	⋯	HiBAL
J164152.2+305851	2.000	−27.2	32.4	1.01	+0.5	51009	52781-1340-073	55832-5201-0914	1.62	4.40	⋯	⋯	LoBAL
J165543.2+394519	1.747	−27.5	32.8	1.38	−0.2	51009	52079-0633-353	56098-6063-0438	1.07	5.08	⋯	⋯	HiBAL[a]

Note. (2)–(5): redshift (z), absolute B magnitude (M_B), radio luminosity (ergs cm^{-2} s^{-1} Hz^{-1}) at a rest-frame frequency of 5 GHz ($\log L_R$), and K-corrected 5 GHz radio to 2500 Å optical luminosity ratio ($\log R^*$) from White et al. (2000). (6): Spectral index between 3.6 and 20 cm ($F_\nu \propto \nu^\alpha$) from Becker et al. (2000). (7)–(9): modified Julian Date of the FBQS and follow-up observations, MJD = JD-2400000. We also present their plate and fiber, if the follow-up spectra come from the SDSS. (10)–(11): rest-frame years of the second and third epoch since the FBQS epoch. (12)–(13): variance of observed magnitudes (Σ_V) and the intrinsic amplitude (σ_V) in the V band calculated by the formalism in Ai et al. (2010).
[a] typical BAL variability.
[b] strong BAL variability.
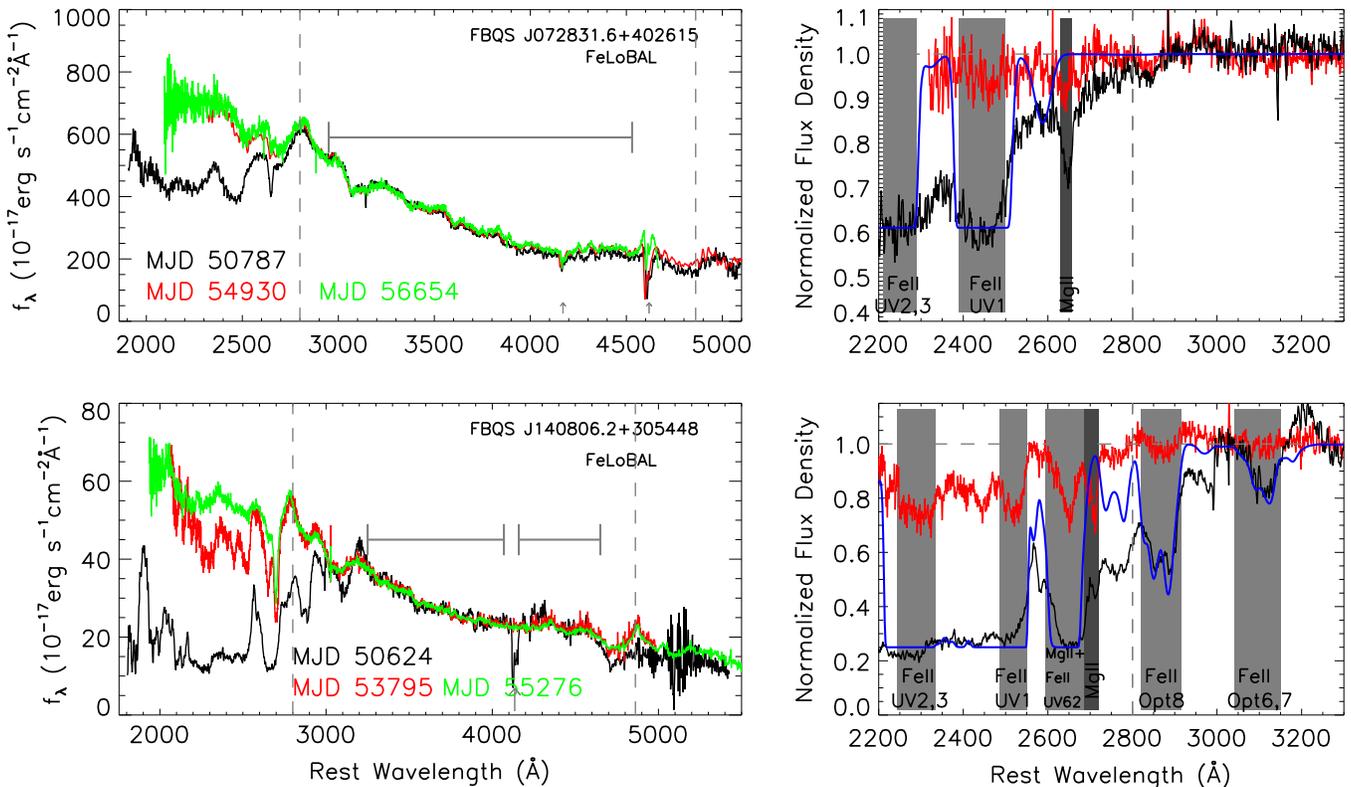
Figure 1. Left: multi-epoch observations of FBQS J072831.6+402615 and J140806.2+305448 in quasar's rest-frame. In each panel, a flux scale is applied to the repeated spectra to match the FBQS spectra in the continuum, and spectra have been smoothed with a three pixel boxcar. Solid horizontal lines show the wavelength coverages used in the spectrum scaled fitting. Dashed vertical lines show the wavelengths of emission from Hβ and Mg II. Note that most FBQS spectra have atmospheric absorption at ~6880 and 7620 Å, masked by the arrows in the panels. Right: difference spectra obtained from the corresponding spectra normalized by the highest fluxes of multi-epoch observations. Dark gray shaded region shows the wavelength range of low-velocity Mg II absorption. Light gray shaded regions show the wavelength ranges absorbed by Fe II multiplets UV1 and UV2+3 and by a blend of Fe II UV62 and high-velocity Mg II absorption. Normalized model profiles for individual photoionization models broadened using Gaussian profile are also displayed by blue curves.

quasar in the repeated spectroscopic observations of these quasars. For FBQS J072831.6+402615, its spectrum from the FBQS epoch contains strong absorption lines from Mg II and Fe II multiplets, with a blueshifted velocity of ~16,000 km s^{-1}. In the OMR spectrum acquired 6.85 rest-frame years later, the absorption troughs of Mg II and Fe II UV1 and UV2+3 had decreased in absorption depth by a factor of four. After an additional 2.88 rest-frame years, the residual overlapping troughs had completely disappeared in the YFOS spectrum. FBQS J140806.2+305448 was a spectacular OFeLoBAL quasar with a covering fraction of Fe II absorption of ~75%, but now, it is only a modestly absorbing LoBAL quasar. Hall et al. (2011) have found there was no significant absorption variability in early observations, one rest-frame year prior to the KECK/ESI observation in 2000 March; however, the Mg II trough outflowing at 12,000 km s^{-1}decreased by a factor of two, and Fe II troughs at the same velocity disappeared over the next ~7 rest-frame years. The SDSS DR10 spectrum shows a complete lack of Fe II troughs (see also the HET spectrum in Hall et al. 2011).

The top panels of Figure 2 show that the three spectra of FBQS J152350.4+391404 are similar to the intermediate epochs of FBQS J140806.2+305448, especially the KECK/ESI spectrum (MJD 53377; Hall et al. 2011). Troughs of Fe II multiplets are clearly visible in all three epochs. The difference spectra reveal strong variability in the ultraviolet Fe II multiplets (Fe II UV1 and UV2+3) and very slight variations in the optical Fe II multiplets (Fe II Opt8 and Opt6+7). Meanwhile,

the red-band spectrographs of the SDSS and BOSS captured a highly blueshifted velocity and an extremely broad absorption trough of Hβ at approximately 4700 Å in the SDSS DR7 and DR10 spectra. Furthermore, a near-infrared spectrum that is quasi-simultaneous with the SDSS DR10 spectrum, which was acquired by the TripleSpec spectrograph of the Hale 200 inch telescope at Palomar Observatory, suggests the existence of Hα BALs. The bottom panels present the observed spectra of the Hβ and Hα regimes overlaid with the best-fit models and the normalized spectra of the blueshifted Balmer absorption troughs. The fitting procedure has been described in detail by Dong et al. (2008); therefore, we outline it only briefly here. The optical continuum from 3600 Å to 6900 Å is approximated by a single power law. Fe II emission multiplets, both broad and narrow, are modeled using the I Zw one template provided by Véron-Cetty et al. (2004). The emission lines are modeled as multiple Gaussians: two Gaussians for broad Balmer lines, and one Gaussian for [O III].

As shown in Figure 3, the BALs of Fe II multiplets are ambiguous or severely overlapped in FBQS J105528.8 +312411 and J140800.4+345125. The spectral variability in these two cases is deepening overall below Mg II and blueward. It is difficult to resolve the absorption multiplets based on their single observations, but it is possible to identify strong variations of the iron multiplets in their difference spectra. The triple-epoch spectra of FBQS J105528.8+312411 reveal that the Mg II BALs are nearly saturated and exhibit no shift. The absorption structures are somewhat similar to those of
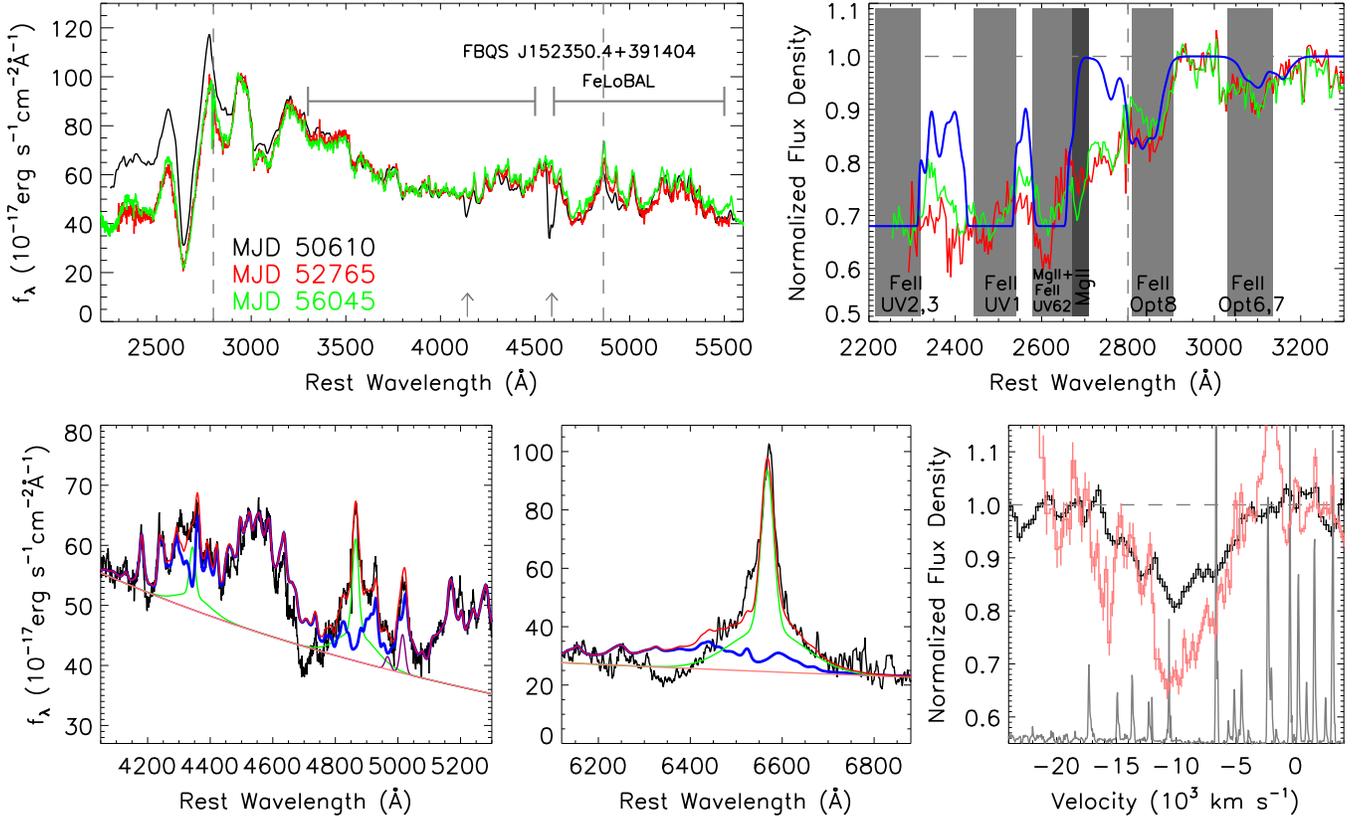
Figure 2. Top panels: as in Figure 1, but showing FBQS J152350.4+391404. Bottom panels: observed spectra of Hβ and Hα regimes overplayed with the best-fit models and normalized spectra of Balmer absorption troughs for FBQS J152350.4+391404. In bottom left and middle panels, we plot the observed spectrum in black curves, power-law continuum in pink, broadened Fe II template in blue, Gaussian Balmer emission lines in green, Gaussian O III emission lines in purple, and the model sum in red. In bottom right panel, the normalized spectra are obtained by dividing the observed spectra by the model spectra. The gray dotted line means the value equals one. Sky line spectrum (not to scale) around Hα is plotted for comparison.

FBQS J140806.2+305448 and J152350.4+391404. We present the identification of the ultraviolet and optical Fe II multiplets in the difference spectra. For FBQS J140800.4+345125, we identify the absorption troughs of Mg II, Al III, and Fe II UV1 (perhaps higher-velocity Mg II) in the FBQS spectrum and mark them by blue diagonal line regions. However, the residual fluxes of the three troughs are constant in all epochs. The normalized fluxes of these troughs in the difference spectra are ~1. This broad absorption line system is invariant. In addition, there are other broad-band absorption troughs in the difference spectra blueward of the invariant absorption troughs noted above, which are surmised to represent the variable absorption of Fe II UV62, UV1 and UV2+3 with the same blueshifted velocity as the invariant absorption system; the iron absorption should be completely overlapping. Another possible explanation is that the Fe II absorption may be undetected in the later spectra of FBQS J105528.8+312411 and J140800.4+345125. The absorption variability may be an illusion caused by a variation in the strength of the Fe II emission, or the apparent overlapping-trough absorption may instead be attributable to reddening changes in the unusual reddening curves, which may cause a rapid dropoff in the flux below a certain wavelength (e.g., Leighly et al. 2014).

4. SUMMARY AND DISCUSSION

In this work, we constructed a radio-selected BAL quasar sample from the FBQS, including 28 reclassified BALs, and also considered subsequent spectroscopic observations of these

quasars from the SDSS and two other instruments to explore the BAL variability among their dual-/triple-epoch spectroscopic observations. Of the investigated sample, 27 BAL quasars were observed in at least one epoch in the SDSS, and follow-up observations of 2 additional quasars were obtained. When we scaled the subsequently acquired spectra to match the continua of the FBQS spectra using a power-law form, we detected variable absorption troughs in 12 BAL quasars through the spectral comparison, including 5 BAL quasars with strong variations in the BALs of Fe II multiplets. Intriguingly, all strong BAL variations were detected in OFeLoBALs; however, other BALs, either with typical variations or without variations, were non-OFeLoBALs.

The apparently opposite trend was observed by Vivek et al. (2012, 2014); in that study, FeLoBALs were found to be less variable than HiBALs and LoBALs. Vivek et al. (2012) probed the time variability of five FeLoBALs spanning an interval of up to 10 yr but only detected strong variations of Fe II UV34 and UV48 in the spectra of SDSS J221511.93-004549.9. Based on photoionization models, de Kool et al. (2002b) showed that an Fe III column density that is higher than that of Fe II can be easily produced in a high-density outflow ($n_e \geqslant 10^{10.5}$ cm^{-3} for an ionization parameter of $U \simeq 10^{-2}$). However, the remaining four FeLoBALs did not exhibit any significant changes either in optical depth or in velocity structure. Two of them, according to studies of their high-resolution spectra performed with VLT and KECK/HIRES, suggested an electron density of $10^{3.3 \pm 0.2}$ cm^{-3} with a distance from the continuum emission
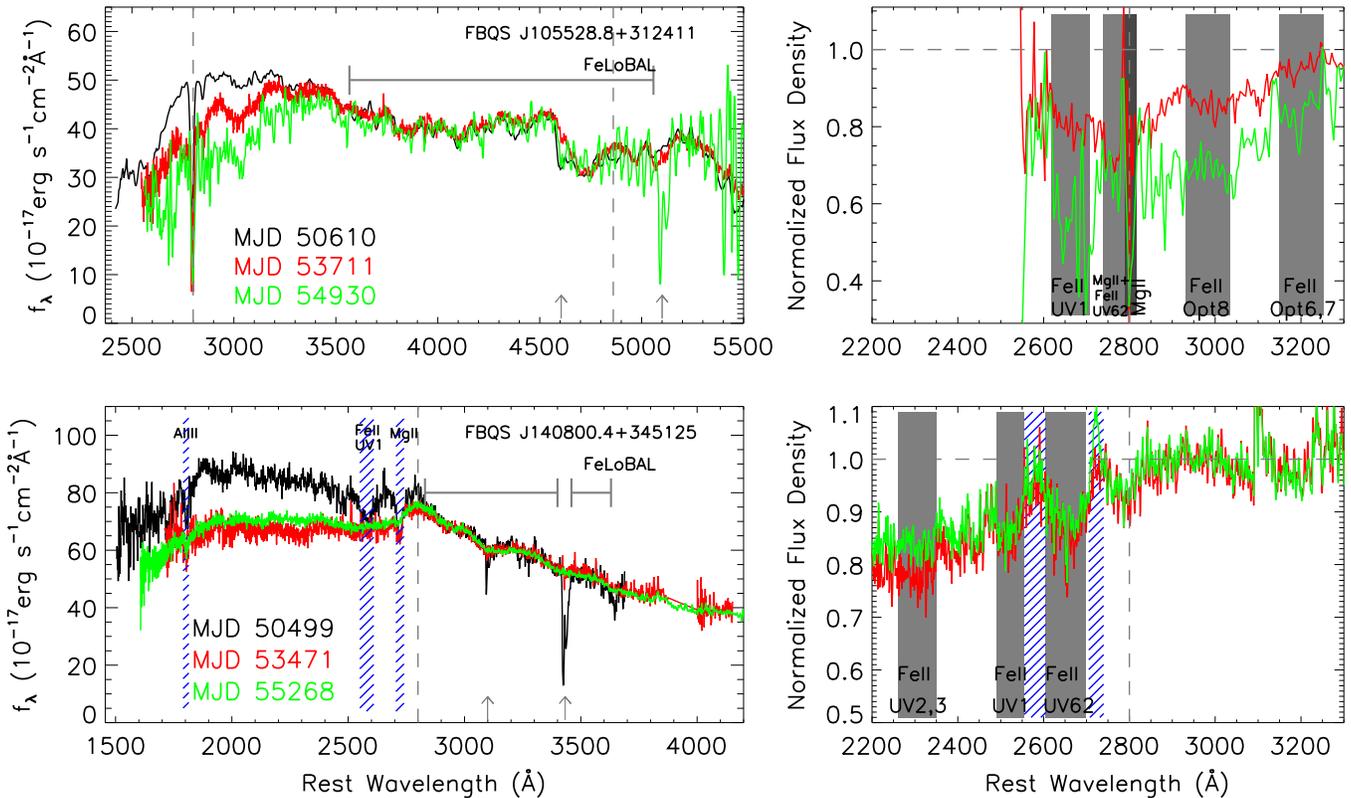
Figure 3. As in Figure 1, but showing FBQS J105528.8+12411 and J140800.4+345125. For FBQS J140800.4+345125, we also present the invariable broad absorption line system by blue diagonal lines.

source of 6 ± 3 kpc for SDSS J031856.62-060037.7 (Dunn et al. 2010) and $n_e \leqslant 500$ cm^{-3} with $D \sim 230$ pc for SDSS J084044.41+363327.8 (de Kool et al. 2002b, also included in this work.).

For the five OFeLoBALs with strong variations studied in this work, the physical properties of the outflow gas are different. In the rotating outflow model, the trough variability arises from a structure in the BAL outflow moving out of our line of sight to the ultraviolet-continuum-emitting region of the quasar's accretion disk. Based on the size of that region and the time scale over which the absorption changes, Filiz Ak et al. (2012) constrained the BAL structure of FBQS J140806.2 +305448 to a transverse velocity between 2600 and 22,000 km s^{-1} and a line of sight velocity of 12,000 km s^{-1}; thus, the moving BAL structure was considered to be located approximately 1.7–14 pc from the black hole, nearly ten to ninety times farther than the Hβ broad-line region. Meanwhile, the application of the large-scale spectral synthesis code CLOUDY (c10.00; Ferland et al. 1998) in the extensive parameter space suggests that the absorbers of all OFeLoBALs considered in this work are ionized gases with a density of $\geqslant 10^6$ cm^{-3} and a column density of $\geqslant 10^{22}$ cm^{-2}. The absorbers in FBQS J140806.2+305448 and J152350.4+391404 are located at distances from the subparsec scale to dozens of parsecs. For FBQS J072831.6+402615, we can provide only an upper limit of $\sim$447 pc, with considerable uncertainty. More details can be found in Appendix. Similarly, McGraw et al. (2014) detected the BAL variability of low-ionization species (Fe II and Mg II) in four objects with a representative upper limit on the distance of the absorber from the center engines of $\sim$20 pc, with crossing speeds of $\gtrsim$500 km s^{-1}.

For the remaining FeLoBALs considered in this work, previous works have reported different locations for the outflow gas. De Kool et al. (2002b) have suggested that the BAL absorbers in FBQS J084044.4+363328 consist of a high-velocity, low-density gas and that the scale of the distance from the black hole is 200 parseconds. Analyses of the KECK/ HIRES spectra of FBQS J104459.5+365605 and J121442.3 +280329 have placed the outflow gas of the Fe II absorbers at distances from the nucleus of 700 pc, with ne $\sim$4 $\times$ 10^4 cm^{-3}, and 130 pc, with $n_e > 10^6$ cm^{-3}, respectively (de Kool et al. 2001, 2002a). For other FeLoBALs, specifically non-overlapping FeLoBALs (non-OFeLoBALs), in the literature, the typical distances between the outflow gas and the nucleus have been derived to be approximately 3–28 kpc (3C 191, Hamann et al. 2001; QSO J2359-1241, Korista et al. 2008; SDSS J0838+2955, Moe et al. 2009; SDSS J0318-0600, Dunn et al. 2010; collected in Table 4 of Lucy et al. 2014).

Above all, FeLoBALs with strong variations are constrained to be located in regions of high density ($\sim$10^6 − 10^9 cm^{-3}) and close to the continuum ionization sources (the upper limit is generally dozens of times farther than the size of the broad-emission-line region). However, the absorbers of other FeLoBALs consist of low-density gas ($<$10^6 cm^{-3}) and are located at distances of hundreds to thousands of parsecs from the central black holes. In other words, the former are located in active galactic nucleus (AGN) environments rather than in the host galaxy. Two subgroups, i.e., FeLoBALs with and without strong BAL variations, may represent the bimodality of Fe II absorption observed by de Kool et al. (2002b). Our findings regarding the different BAL variability behaviors of these two FeLoBAL subgroups suggest that they also correspond to
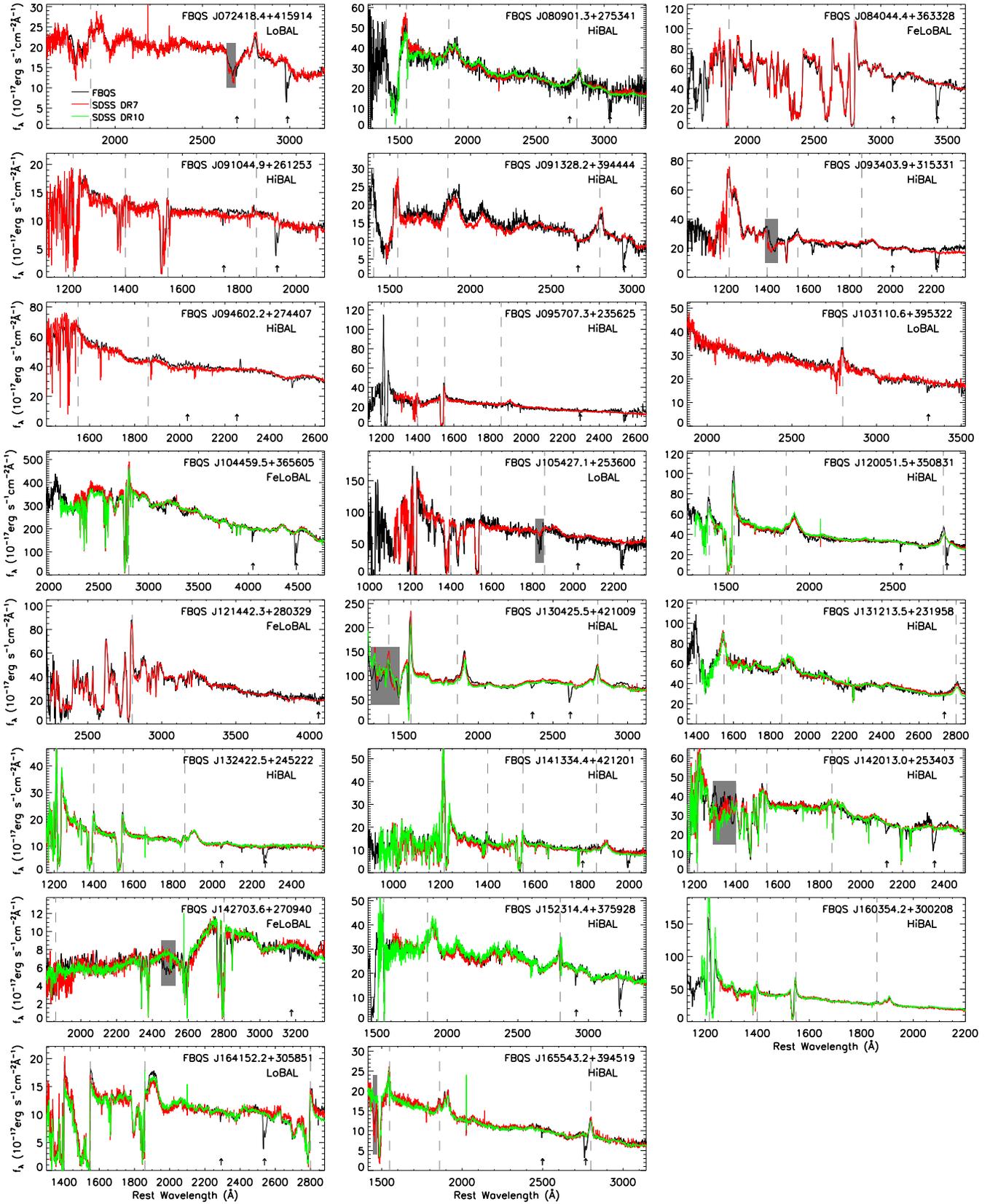
Figure 4. Multi-epoch observations of 7 typical BAL variations and 16 invariable BALs in the quasar's rest-frame. In each panel, flux scale applies to the repeated spectra to match the FBQS spectra in continuum and spectra have been smoothed with a three-pixel boxcar. Dashed vertical lines show the wavelengths of emission from Lyα, Si IV, C IV, Al III, and Al Mg II. Arrows mask the potential atmospheric absorption at ∼6880 and 7620 Å in the panels. Gray shaded regions mark variable BALs for each measurement.
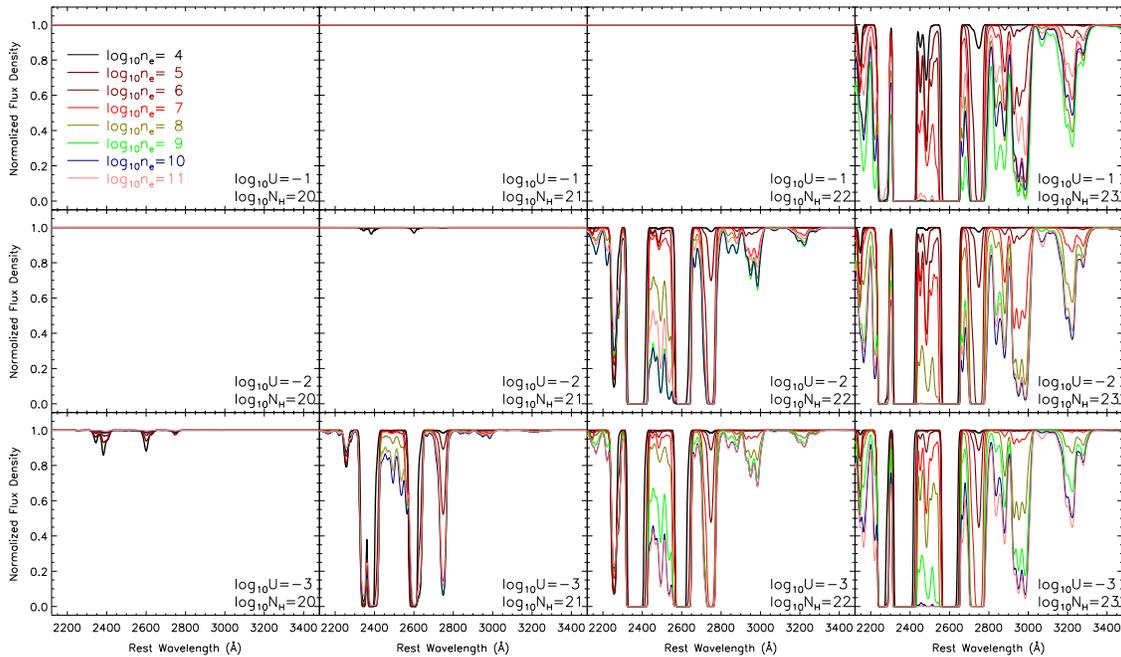
Figure A1. Normalized spectra of Fe II absorption lines in the 2100–3500 Å region predicted by the model using CLOUDY. In panels, the blueshift velocity of each Fe II absorption line is set to 0 km s^{-1}, and their widths are 2000 km s^{-1}.

overlapping and non-overlapping FeLoBALs. If our hypothesis is correct, then OFeLoBALs correspond to densities that are "higher by several orders of magnitude than in the absorbers in the "low-density gas at a large distance" group", and "their properties are best explained if they are 1000 times closer to the nucleus" (de Kool et al. 2002b). On the other hand, we suggest that a high density of the absorbing gas and a large width of the absorption lines are the necessary conditions for OFeLoBALs (Hall et al. 2002). A higher density implies that the absorbing gas should be located closer to the central engine, and higher densities and broader absorption lines certainly require smaller BALs; these conditions are certainly consistent with the necessary conditions for variable BALs. The above estimations of the gas density and distance of strongly variable FeLoBALs are in good agreement with the requirements for OFeLoBALs. This is the reason why strong BAL variations are detected only in OFeLoBALs.

The possible geometries and origins (Arav et al. 1994; de Kool & Begelman 1995; Murray et al. 1995; Elvis 2000) imply that the variability of the BALs is explained by variations in the ionizing flux originating in the inner part of the accretion disk (e.g., Netzer et al. 2002; Trevese et al. 2013) and a transiting structure in the BAL outflow (e.g., Risaliti et al. 2002; Hall et al. 2011). The very optically thick gas that is required for OFeLoBALs is very unlikely to undergo any change in ionization that is sufficiently large for the gas to become only slightly optically thick and thus exhibit a detectable response to ionizing-continuum variability. Meanwhile, the 9 yr of monitoring performed by the Catalina Surveys (Drake et al. 2014), beginning in 2005 April, shows there is no apparent change in the optical continuum, at least in the V band, for these OFeLoBAL quasars (Table 1). However, we cannot definitively rule out a change in the ionizing flux as the explanation for the strong variability of the Fe II absorption. Observations in the V band do not reflect the change in extreme UV and soft X-ray photons at $\lambda \lesssim 912$ Å; moreover, the ionizing and observed

continua along our line of sight may not always track each other (Kaastra et al. 2014). If the BAL variability is related to the transverse motions of flows, then a large transverse velocity is required to produce such variability on a relatively short time scale, and the absorbing gas must be close to the black hole in a rotating disk wind model. This analysis agrees with Hall et al. (2011) that the strong BAL variability is possibly attributable to variability in the covering factor of BAL regions caused by clouds transiting across the line of sight rather than to ionization variations. We also note that three of the four OFeLoBAL quasars for which there are measurements of the radio spectral index are steep-spectrum radio sources, and the remaining one (FBQS J152350.4+391404) has a radio spectral index of $\alpha = -0.4$, falling close to the dividing line, $-0.6 \leqslant \alpha \leqslant -0.4$ (Becker et al. 2000). The steep radio spectra suggest that these quasars should be regarded as lobe-dominated radio sources that are viewed at larger angles. This is also consistent with the interpretation of the strong BAL variations based on the rotating outflow model.

APPENDIX
PHYSICAL PROPERTY ESTIMATION OF THE IRON ABSORBERS

The OFeLoBALs considered in this work are severely overlapping; thus, the geometry and physical conditions of the outflow winds cannot be accurately obtained through analysis of the combination of the absorption lines. Fortunately, we can approximately evaluate the BALs by employing the large-scale spectral synthesis code CLOUDY (c10.00; Ferland et al. 1998) in the extensive parameter space. In the photoionization simulation, the geometry is assumed as a slab-shaped absorbing medium exposed to the ionizing continuum from the central engine with a uniform density, metallicity, and abundance pattern. A typical AGS multi-component continuum from Mathews & Ferland (1987) is specified as the incident ionizing radiation. The solar elemental abundance is adopted, and the gas is assumed to be free of dust. Each individual simulation model is customized in terms of the ionization parameter (U), electron density (n_e) and hydrogen column density (N_H). The variation ranges in $U - n_e - N_H$ space are $3 \leqslant \log 10U \leqslant 0$, $4 \leqslant \log 10 \, n_e \, (cm^{-3}) \leqslant 11$, and $20 \leqslant \log 10N_H \, (cm^{-2}) \leqslant 23$, with a dex step of 1.0. The full 371-level Fe^+ model implemented in CLOUDY, which includes all levels up to 11.6 eV, is used to reproduce the Fe II absorption. The employed model can predict the populations of various levels of Fe^+ and the strengths of the absorption lines arising from these levels.

Figure A1 presents a series of models in $U - n_e - N_H$ space. To clearly illustrate the trend, one Gaussian profile, with its FWHM set to 2000 km s^{-1}, is used to visualize the models. The calculations suggest that the iron multiplets raised from the ground state (e.g., Fe II UV2+3 at approximately 2400 Å and Fe II UV1 at approximately 2600 Å) are the most pervasive and that they are even generally saturated when the outflow winds have high column densities. However, the iron multiplets that are raised from the excited state (e.g., Fe II UV144-149 and UV158-164 in the wavelength range of 2462-2530 Å as well as Fe II Opt6+7 and Opt8) are more sensitive to the selected parameters. The iron absorption troughs increase with increasing Fe^+ density, as determined by the combination of the ionization parameter, the electron density and the hydrogen column density. Moreover, for larger U or n_e, more Fe^+ will become ionized to Fe^{2+}, and the absorption troughs of the high multiplets Fe II UV144-149 and UV158-164 as well as Fe II Opt6+7 and Opt8 will become even weaker. We can

approximately limit the physical parameters of the outflow winds based on the absorption strength/depth ratios of the Fe II UV1 and UV2+3 multiplets, the Fe II UV144-149 and UV158-164 multiplets, the Fe II UV1 and UV2+3 multiplets, and the Fe II Opt8 multiplets as is done for the estimation of the strength ratios of Fe II emission multiplets in Baldwin et al. (2004). The Fe II UV144-149 and UV158-164 multiplets in the four OFeLoBALs (with the exception of FBQS J105528.8 +312411) that are considered in this work have depths that are nearly identical to those of the troughs of Fe II UV1 and UV2 +3, and in three cases, considerable absorption troughs of Fe II Opt6+7 and Opt8 are evident. These characteristics suggest that the outflow winds of OFeLoBALs should be of high density ($n_e \geqslant 10^6 \, cm^{-3}$) and high column density ($N_H \geqslant 10^{22} \, cm^{-2}$).

For individual sources with relatively isolated absorption multiplets, we attempt to match the observed maximal difference spectra using photoionization models with appropriate broadening widths and blueshifted velocities. The covering factor is set to the average depths of Fe II UV1 and UV2+3. In the search for optimal photoionization models, the reduced two is evaluated using data covering absorption rest frames of 2300 to 3400 Å, which contain the overall absorption features of the Fe II multiplets mentioned above. Because the photoionization simulations are performed on a large grid, the physical parameters of the optimal models are determined through approximation, and a simulation using incremental grids will accurately evaluate the observations. In the right-hand panels of Figure 1 and the top-right panel of Figure 2, the best-matched photoionization models for the observed difference spectra are represented by blue curves. For FBQS J140806.2+305448, a model with $U = 10^{-1}$, $n_e = 10^{11} \, cm^{-3}$, $N_H = 10^{23} \, cm^{-2}$, and FWHM = 2000 km s^{-1} exhibits absorption features that are quite consistent with the observations, with the exception of the absorption between the troughs of Mg II and Fe II Opt8. The underestimation of the absorption at approximately 2850 Å is attributed to Cr II λ2835, 2840, 2849, 2860, 2867, and Mg I λ2851 (X. L Shi et al., in preparation). Similarly, a model with $U = 10^{-2}$, $n_e = 10^7 \, cm^{-3}$, $N_H = 10^{23} \, cm^{-2}$, and FWHM = 3000 km s^{-1} is the optimal photoionization model for FBQS J152350.4+391404, and there are also obvious Cr II absorption lines present at approximately 2850 Å in the difference spectra. Using the ionization parameter definitions and the inferred values of the ionization photon emission rate, ionization parameter, and density, one can determine the distance of the outflow winds from the central ionization source, which is found to be $R_{BAL} \sim 0.16$ pc for FBQS J140806.2+305448 and 34 pc for FBQS J152350.4 +391404. Based on the absorption depths of Fe II UV1 and UV2+3 and possibly Fe II UV62, we obtain a model spectrum using $U = 10^{-3}$, $n_e = 10^6 \, cm^{-3}$, and $N_H = 10^{22} \, cm^{-2}$ to match the difference spectrum of FBQS J072831.6+402615; the distance of the outflow winds is then found to be ~447 pc. However, the difference spectra of FBQS J152350.4+391404 and J072831.6+402615 indicate stronger absorption of the Fe II UV144-149 and UV158-164 multiplets than is present in the optimal models, which most likely suggests a higher density and a higher ionization parameter or some microturbulence in the outflow winds (Shi et al. 2015). If the density and/or ionization parameters of these two cases are underestimated, then the absorbing gas should be located closer to the ionization continuum sources than our estimates indicate.

REFERENCES

Abazajian, K. N., Adelman-McCarthy, J. K., Agüeros, M. A., et al. 2009, ApJS, 182, 543
Ahn, C. P., Alexandroff, R., Allende Prieto, C., et al. 2014, ApJS, 211, 17
Ai, Y. L., Yuan, W., Zhou, H. Y., et al. 2010, ApJl, 716, L31
Arav, N., Li, Z.-Y., & Begelman, M. C. 1994, ApJ, 432, 62
Baldwin, J. A., Ferland, G. J., Korista, K. T., Hamann, F., & LaCluyzé, A. 2004, ApJ, 615, 610
Becker, R. H., Gregg, M. D., Hook, I. M., et al. 1997, ApJl, 479, L93
Becker, R. H., White, R. L., Gregg, M. D., et al. 2000, ApJ, 538, 72
Capellupo, D. M., Hamann, F., Shields, J. C., Halpern, J. P., & Barlow, T. A. 2013, MNRAS, 429, 1872
Capellupo, D. M., Hamann, F., Shields, J. C., Rodríguez Hidalgo, P., & Barlow, T. A. 2011, MNRAS, 413, 908
Capellupo, D. M., Hamann, F., Shields, J. C., Rodríguez Hidalgo, P., & Barlow, T. A. 2012, MNRAS, 422, 3249
de Kool, M., Arav, N., Becker, R. H., et al. 2001, ApJ, 548, 609
de Kool, M., Becker, R. H., Arav, N., Gregg, M. D., & White, R. L. 2002b, ApJ, 570, 514
de Kool, M., Becker, R. H., Gregg, M. D., White, R. L., & Arav, N. 2002a, ApJ, 567, 58
de Kool, M., & Begelman, M. C. 1995, ApJ, 455, 448
DiPompeo, M. A., Brotherton, M. S., & de Breuck, C. 2012, ApJ, 752, 6
Dong, X., Wang, T., Wang, J., et al. 2008, MNRAS, 383, 581
Drake, A. J., Graham, M. J., Djorgovski, S. G., et al. 2014, ApJS, 213, 9
Dunn, J. P., Bautista, M., Arav, N., et al. 2010, ApJ, 709, 611
Elvis, M. 2000, ApJ, 545, 63
Ferland, G. J., Korista, K. T., Verner, D. A., et al. 1998, PASP, 110, 761
Filiz, Ak, N., Brandt, W. N., Hall, P. B., et al. 2012, ApJ, 757, 114
Filiz, Ak, N., Brandt, W. N., Hall, P. B., et al. 2013, ApJ, 777, 168
Gibson, R. R., Brandt, W. N., Schneider, D. P., & Gallagher, S. C. 2008, ApJ, 675, 985
Gibson, R. R., Jiang, L., Brandt, W. N., et al. 2009, ApJ, 692, 758
Gibson, R. R., Brandt, W. N., Gallagher, S. C., Hewett, P. C., & Schneider, D. P. 2010, ApJ, 713, 220
Hall, P. B., Anderson, S. F., Strauss, M. A., et al. 2002, ApJS, 141, 267
Hall, P. B., Anosov, K., White, R. L., et al. 2011, MNRAS, 411, 2653
Hamann, F. W., Barlow, T. A., Chaffee, F. C., Foltz, C. B., & Weymann, R. J. 2001, ApJ, 550, 142
Hazard, C., McMahon, R. G., Webb, J. K., & Morton, D. C. 1987, ApJ, 323, 263
Joshi, R., Chand, H., Srianand, R., & Majumdar, J. 2014, MNRAS, 442, 862
Kaastra, J. S., Kriss, G. A., Cappi, M., et al. 2014, Science, 345, 64
Korista, K. T., Bautista, M. A., Arav, N., et al. 2008, ApJ, 688, 108
Leighly, K. M., Terndrup, D. M., Baron, E., et al. 2014, ApJ, 788, 123
Lucy, A. B., Leighly, K. M., Terndrup, D. M., Dietrich, M., & Gallagher, S. C. 2014, ApJ, 783, 58
Lundgren, B. F., Wilhite, B. C., Brunner, R. J., et al. 2007, ApJ, 656, 73
Mathews, W. G., & Ferland, G. J. 1987, ApJ, 323, 456
McGraw, S. M., Shields, J. C., Hamann, F. W., et al. 2014, in IAU Symp., 304, Multiwavelength AGN Surveys and Studies (Cambridge: Cambridge Univ. Press), 417
Moe, M., Arav, N., Bautista, M. A., & Korista, K. T. 2009, ApJ, 706, 525
Murray, N., Chiang, J., Grossman, S. A., & Voit, G. M. 1995, ApJ, 451, 498
Netzer, H., Chelouche, D., George, I. M., et al. 2002, ApJ, 571, 256
Reichard, T. A., Richards, G. T., Hall, P. B., et al. 2003, AJ, 126, 2594
Risaliti, G., Elvis, M., & Nicastro, F. 2002, ApJ, 571, 234
Smee, S. A., Gunn, J. E., Uomoto, A., et al. 2013, AJ, 146, 32
Trevese, D., Saturni, F. G., Vagnetti, F., et al. 2013, A&A, 557, AA91
Trump, J. R., Hall, P. B., Reichard, T. A., et al. 2006, ApJS, 165, 1
Véron-Cetty, M.-P., Joly, M., & Véron, P. 2004, A&A, 417, 515
Vivek, M., Srianand, R., Petitjean, P., et al. 2012, MNRAS, 423, 2879
Vivek, M., Srianand, R., Petitjean, P., et al. 2014, MNRAS, 440, 799
York, D. G., Adelman, J., Anderson, J. E., Jr., et al. 2000, AJ, 120, 1579
Welling, C. A., et al. 2014, MNRAS, 440, 2474
Weymann, R. J., Morris, S. L., Foltz, C. B., & Hewett, P. C. 1991, ApJ, 373, 23
White, R. L., Becker, R. H., Gregg, M. D., et al. 2000, ApJS, 126, 133
Zhang, S., Wang, T.-G., Wang, H., et al. 2010, ApJ, 714, 367
Zhang, S.-H., Wang, H.-Y., Zhou, H.-Y., Wang, T.-G., & Jiang, P. 2011, RAA, 11, 1163
Zhou, H., Wang, T., Wang, H., Wang, J., Yuan, W., & Lu, Y. 2006, ApJ, 639, 716